Optical Trapping with Integrated Near-Field Apertures

Eun-Soo Kwak,[†,‡] Tiberiu-Dan Onuta,[†,‡] Dragos Amarie,[†,§] Radislav Potyrailo,[||] Barry Stein,[⊥] Stephen C. Jacobson,[‡] W. L. Schaich,[§] and Bogdan Dragnea*[,‡]

Departments of Chemistry and Physics, Indiana University, Bloomington, Indiana 47405, GE Global Research Center, Schenectady, New York, and Indiana Molecular Biology Institute, Indiana University, Bloomington, Indiana 47405

Received: May 7, 2004; In Final Form: June 16, 2004

In recent years, optical micromachines based on forces exerted by strongly focused beams of light have started to provide unprecedented access to nonintrusive measurement and manipulation of matter on submicron length scales. However, the sharpness of the present optical tweezers is restricted by the spatial gradients of light attainable with diffraction-limited optics. Here, we demonstrate a technique for optical trapping of single particles in a fluid, which is based on the intense near-field gradients around small apertures in a metal film. Our scheme should be able to trap smaller particles with a fraction of the laser intensity required by conventional optical tweezers. Detailed simulations of the electromagnetic fields near apertures and the resulting forces they can produce are described. We also present a proof-of-principle experiment in which the trapping of latex beads is demonstrated by following the time evolution of their fluorescence. Our scheme allows containment of particles in free solution in nanometer sized "beakers" opening the way for research on single nanoparticle chemistry, microrheology in confined environments, and ultrahigh sensitivity sensors.

Introduction

When a small particle with an index of refraction greater than that of its environment moves near the waist of a focused beam of light, forces resulting from the scattering of photons on different regions of the particle tend to immobilize it in the most intense part of the focal zone, i.e., the center. The optical force can exceed room-temperature Brownian forces if the field gradient across the diameter of the particle is strong enough. This method of three-dimensional position control of a particle in a fluid, known as optical tweezers, has led to an enormous number of applications ranging from the fundamental physics of ultracold atoms to subcellular dynamics.[1−5] The wide acceptance gained by optical tweezers in the biology community,[3,6] greater than by any other proximity probe technique, is due to its nonintrusiveness, quasi three-dimensional character, and capability of measuring the very small forces, 10^{-13} to 10^{-10} N, relevant for biological matter.[6] However, the requirement of a strong gradient of light intensity across the particle implies that particles smaller than the diffraction limit (∼250 nm) are difficult to trap. Because of this limitation, only relatively large viruses, such as the tobacco mosaic virus (∼500 nm in length), can be trapped with light beams mild enough to preserve their integrity.[7,8]

To alleviate the particle size problem, several researchers have proposed use of near-field optical tweezers relying on the strongly enhanced electric fields present close to metal nanostructures.[9−11] The near-field consists of evanescent components, which decay over much shorter distances than the wavelength of the light. In this way, even single molecules in a fluid might be stabilized against Brownian motion.[12,13] This idea, although very promising, has not been realized in practice until now with either aperture-based or apertureless near-field scanning optical microscopes.

Instead of using a near-field microscope tip to catch a nanoparticle, we have used a large ensemble of nanoapertures, or channels, fabricated in a thin metal film. The particles for study are dispersed in a solution in contact with the metal film and some of them diffuse into the channels. When a laser beam is shone onto the metal film, the particles located inside the channels are trapped due to the strong near-field intensity gradients that develop. Although many channels are simultaneously illuminated, they can be "read" one at a time with a confocal scanning microscope from the other side of the film. We can thus choose a trap that was incidentally populated when the laser was turned on.

To avoid irreversible particle adsorption onto the nanochannel walls, the metal surface is functionalized with ionizable chemical groups able to provide a short-range repelling force on any trapped particle. A diluted solution ensures that only a few traps are populated and that there is little chance of a pair of particles being trapped in the same hole. We show here that this scheme of near-field trapping (NFT) within nanochannels in metal films is theoretically employable down to a particle size of 10 nm, and we present the first experimental realization with data highlighting the main characteristics of the NFT approach.

NFT has several unique advantages: (a) possibility of large-scale integration using well-established microlithographic methods, (b) reduction of the observation volume allowing for higher ligand concentrations than those required in traditional single-molecule studies,[14] (c) intrinsic small background due to the confinement of the excitation to the subwavelength metal cavity, (d) field-enhancement by the close proximity of the metal surface, (e) capability of trapping 10-nm particles at biologically tolerable laser intensities, and (f) possibility of massively parallel

* To whom correspondence should be addressed. E-mail: Dragnea@indiana.edu.
[†] These authors contributed equally to this work.
[‡] Department of Chemistry, Indiana University.
[§] Department of Physics, Indiana University.
[||] GE Global Research Center.
[⊥] Indiana Molecular Biology Institute, Indiana University.

10.1021/jp048028a CCC: $27.50
Published on Web 08/18/2004

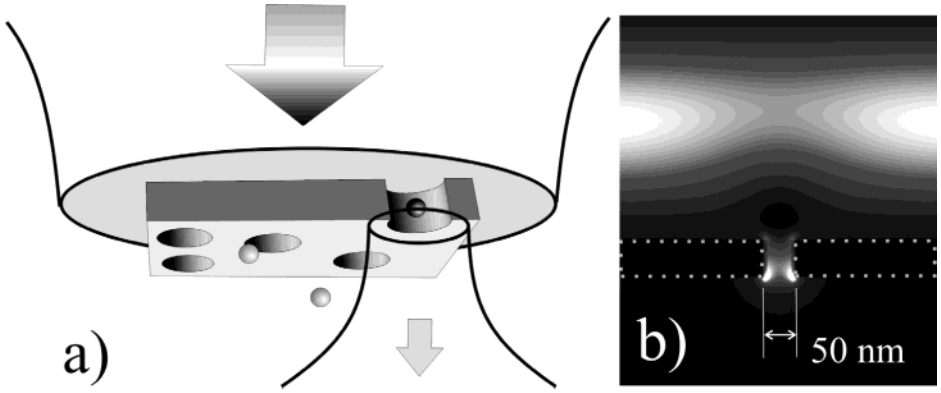

Figure 1. (a) Schematic of the NFT method: the incident beam illuminates from above a few nanoholes in an opaque metal screen. The nanoholes are spaced widely enough to allow single nanohole selection by high numerical aperture collection optics from below. (b) Vertical cross-section with density map of the p-polarized electric field intensity, inside a one-dimensional channel through a 50-nm-thick, free-standing gold film. The laser wavelength is 750 nm.

sensing by integrating many traps on the same chip while using trap transducers with different specificities. We therefore believe that the NFT platform provides a promising basis for future biophotonic sensors with subwavelength-sized structures and new possibilities for ultrasensitive measurements of hydrodynamic properties of particles in confined environments.

NFT Theoretical Considerations

Figure 1a illustrates the aperture-based NFT principles. The main question is whether the trapping force generated on a particle inside a nanochannel is strong enough to overcome Brownian motion and to keep the particle from drifting away. We show in the following that field enhancements and strong intensity gradients are expected to occur inside such a channel, opening the possibility for optical trapping of particles as small as 10 nm diameter. It is essential to perform a detailed electromagnetic analysis to understand and predict the forces inside a near-field optical trap. The result of such a calculation, done by the finite-difference time-domain method (FDTD),[15] is shown in Figure 1b.

For this channel we have analyzed the simple model of an infinitely long slit, 50 nm deep and 50 nm wide. Optical parameters of Au at 750 nm wavelength have been used for the metal film, which is surrounded by vacuum. The calculation is two-dimensional, but it is expected to capture well the essence of the phenomenon since it has worked satisfactorily in discussions of near-field scanning optical microscope apertures.[16,17] A rapid spatial decay of the light intensity in the channel, characteristic for the near-field, can be noticed within ~20 nm from the channel boundaries. With the field distribution inside the channel determined, one can use the dipole approximation for the particle's response to estimate the force induced by the intensity gradient

$$F = \frac{\alpha}{2}\nabla E^2 \qquad (1)$$

where α is the polarizability of the particle.[18]

Now consider a spherical gold particle of 10 nm diameter and an average laser intensity incident on the film of 10^5 W/mm^2, a typical intensity for classical optical tweezers. (Note that this is the light intensity above the film, not inside the channel.) Figure 2 plots the force exerted on the gold particle along the central axis. The force is negative (it points toward the channel) close to the entrance of the aperture for distances smaller than ~100 nm. This means that the nanochannel should act as a funnel for particles undergoing Brownian motion in its

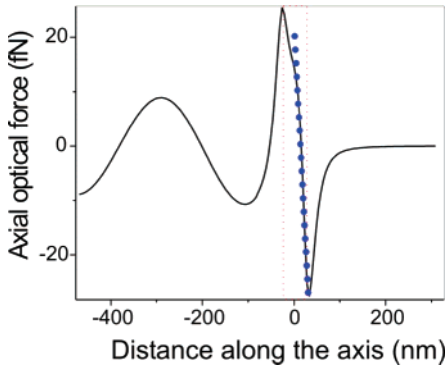

Figure 2. Axial force on a gold particle of 10-nm diameter exerted along a 50-nm-wide channel in a gold film. The laser beam is incident on the film from the left. The film limits are given by the dotted rectangle. The dots represent a linear fit to the restoring force.

vicinity. If we make a linear fit to the restoring force near the top of the channel, we obtain an effective spring constant which, by equipartition, implies a root-mean-square displacement of less than 50 nm; i.e., less than the size of the channel. Only the possibility of axial escape from the trap has been considered here because, as seen in Figure 1b, the maximum gradients are reached close to the metal edges and therefore the particle is most likely to escape along the middle of the channel. Furthermore, the channel walls limit the lateral motion. Trapping of such small particles should therefore be possible.

Because the optical force increases as the cube of the particle diameter while it is only linearly proportional to the intensity of the field, the particles trapped by the nanochannel method will be limited in size to above ~10 nm diameter. However to obtain stable trapping for a 30 nm diameter particle, the incident laser intensity could be reduced to only $\sim 3 \times 10^3$ W/mm^2, at least 2 orders of magnitude less than that for classical optical tweezers. This intensity is low enough to allow, for example, real-time investigations of the self-assembly process of delicate biological nanoparticles such as small virus capsids around trapped nanoparticle cores.[19]

We next describe results from a full, three-dimensional, FDTD calculation for the fields near a hole in a gold film on a glass substrate and immersed in water. With the light incident from the glass side, we show in Figure 3 typical behaviors. An intriguing feature predicted by the theory is a relatively uniform confinement of the light emerging from the aperture for distances comparable to twice the channel diameter. This characteristic predicted by our computations has been directly confirmed experimentally as follows. Nanochannels were fabricated in a

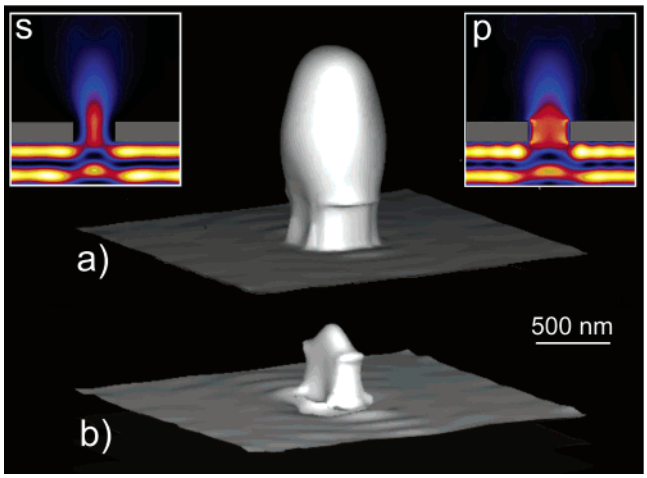

Figure 3. Calculated light iso-intensity surfaces for a 500-nm-diameter channel in a 220-nm film irradiated by an 800-nm-wavelength laser from below. The intensity for the iso-surface in (b) is five times greater than for that in (a). Inset: light intensity profiles within cross-sections cutting through the center of the channel and either in the polarization plane (p), or perpendicular to it (s).

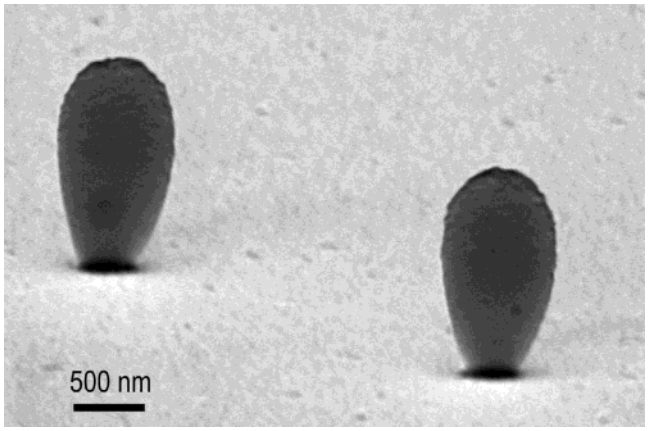

Figure 4. Polymeric resist replica of the light intensity emerging from a near-field aperture. The polymer pillar is ~1.6 μm high. The shape, aspect ratio, and weak divergence are features predicted by the numerical simulations of the iso-intensity surfaces of Figure 3.

250-nm-thick Au film on glass by the nanosphere lithography method.[20] The nanochannel sample was then coated with 10-μm-thick negative tone photoresist layer and the film was exposed from the other side to UV light (300−450 nm, exposure ~10 mJ/cm^2). After developing, the exposed areas of the resist were imaged by scanning electron microscopy (SEM), Figure 4. The cross-linked polymer structures of the exposed areas represent a replica of the exposure iso-intensity surface which corresponds to the polymerization threshold. There is a clear similarity between the polymer replicas in Figure 4 and the simulation in Figure 3a. Another conclusion emerging from this experiment is that the symmetry, smooth surface, and sharp height distribution of the light intensity polymer replicas indicate that the nanosphere lithography is suitable for generating near-field nanochannels with reproducible properties.

It is apparent from Figure 3 that a trapped particle is likely to reside somewhere inside the structure in Figure 3b and will probably be attracted toward one of the two hot-spots on the channel edge which are aligned with the incident electric field polarization. The presence of a material wall with which the trapped particle can interact is another characteristic that distinguishes NFT from the classical optical tweezers. Care must be taken to control this interaction by tuning the surface properties of the channel. In this way, pinning of the particle at the channel edges can be avoided (or utilized, if it turns out to be advantageous).

The horizontal cross-section of the trap shown in Figure 3 for fixed polarization of incident light has a quasi-elliptical shape. This may be smoothed into a circular shape if the field polarization is rapidly rotated around the symmetry axis. One needs only to impose a rotation frequency higher than the cut-off frequency for mechanical response. This is similar to procedures used in ion trap or quadrupolar mass spectrometry in which rotating fields define a time-averaged stable pseudo-potential well.

NFT Experiments with Fluorescent Latex Beads

NFT experiments have been carried out with commercially available 200-nm fluorescent latex beads in water (carboxylate-modified Pt^{2+}-porphyrin FluoSpheres, Molecular Probes, Inc.; excitation maximum 390 nm, emission maximum 650 nm) and 500-nm-diameter nanochannels fabricated in a 250-nm-thick Au film deposited on glass. The Au film has been evaporatively coated at deposition rates larger than 50 Å/s onto a 4-nm-thick Cr adhesion layer. The Au and Cr thicknesses were measured in situ using a calibrated quartz crystal microbalance. The average nanochannel surface density has been chosen to correspond to an average distance of ~50 μm between two nanochannels. This distance is significantly larger than the surface plasmon attenuation length measured for evaporatively coated Au films,[21] and therefore, the holes are not expected to exhibit any electromagnetic coupling via surface waves.[22] Prior to the experiment, the Au film was coated with a self-assembled monolayer of mercaptosuccinic acid.[23] Surface functionalization was routinely checked by FTIR spectroscopy and wetting angle experiments. Without this molecular layer, the experiments described below were not possible, due to irreversible adsorption of the polystyrene (PS) beads on the Au film through probably hydrophobic or van der Waals interactions. NaCl was added to the solution to control the range of electrostatic repulsion between the surface and a bead.

Two light sources have been used: the frequency-doubled output of an ultrafast regenerative amplifier (λ = 400 nm, 300 kHz repetition rate, 150 fs) and a near-infrared Ti/sapphire laser (800 nm, 76 MHz repetition rate, 130 fs). The sample was mounted in a fluid cell in a confocal inverted microscope (Nikon, TE-300 Eclipse) fitted with a piezo-scanning stage (PI-517CL, Polytec PI), a photon-counting avalanche photodiode (SPCM-AQR-16 FC, PerkinElmer Optoelectronics), and an imaging grating spectrometer (300 mm, SpectraPro 300i, Acton Research). Detection of fluorescence from individual nanochannels by the fast avalanche photodiode, instead of changes in transmission, facilitates the realization of a proof-of-principle experiment.

Figure 5 shows successive trapping events recorded by monitoring the fluorescence emitted from a single nanochannel. In this case, the trapping and the excitation laser were the same. When the laser is on, a small fluorescence background (100 cts/s) coming from remote particles passing through the scattered light from the empty aperture can be observed. More than a 3-fold increase in the fluorescence intensity and a characteristic fluctuation pattern accompany the arrival of a particle. Turning off the laser leads to the particle release when the aperture is functionalized with negatively charged moieties. Turning on the laser again leads to a new capture. When the laser intensity is increased to ~30 mW/mm^2, an exponential decay signature (bleaching) indicates a signal coming from a single particle (data

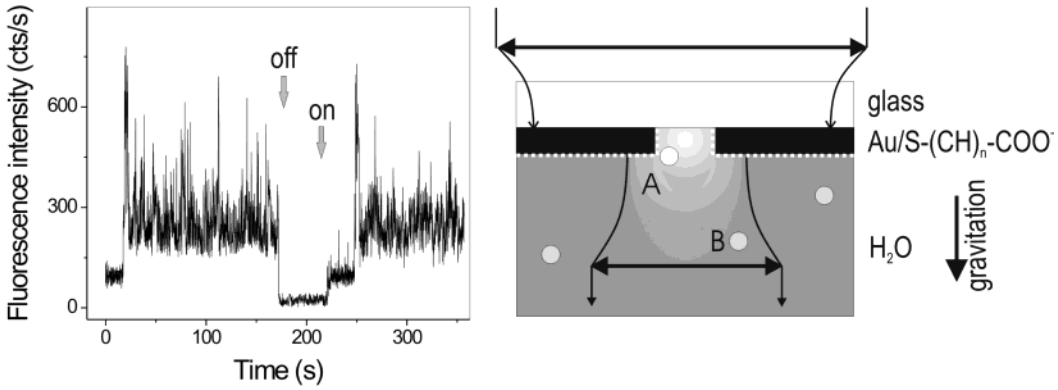

Figure 5. Fluorescence emission recording from a single 500-nm-diameter nanochannel corresponding to the arrival and release of a particle and to the trapping of a new one. The arrows mark the instants of turning off and turning on the laser. The dashed line on the experimental schematic represents a self-assembled molecular layer with the role of preventing the adsorption of carboxylated PS beads onto the Au film. A, emitting particle; and B, particle contributing to the fluorescence background.

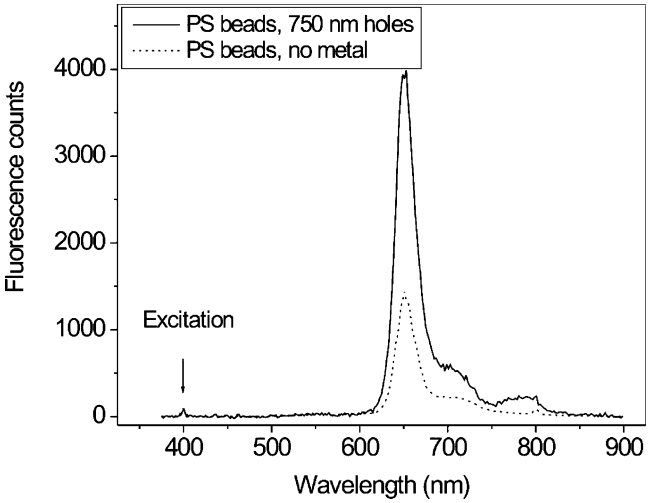

Figure 6. Fluorescence spectra collected from a single bead inside a channel (solid curve) and from a few beads within the confocal volume in the absence of a metal film (dashed curve). The spectra are normalized to the excitation line ($\lambda = 400$ nm).

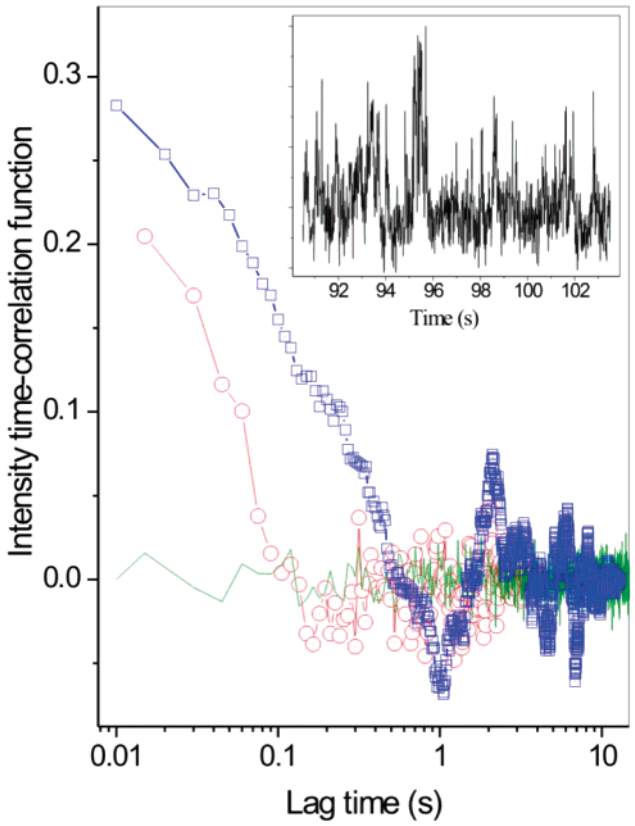

Figure 7. Comparison between the correlation function of fluorescence fluctuations from a trapped bead (open squares), a free bead (open circles), and a fixed (adsorbed) bead (continuous line). Inset: part of the original recording of fluorescence fluctuations for the trapped bead vs time at 10 ms resolution.

not shown). For all other experiments we used lower intensities so that the photochemical decay did not obscure the dynamics of fluorescence fluctuations. At large particle concentrations (~10 times larger than the 0.25 μm^{-3} concentration used in these experiments), the simultaneous arrival of two particles is a possible event; nevertheless, it is easily distinguishable by intensity considerations. In Figure 5, the particle remains confined within the nanochannel for at least 3 min. It would take about 40 ms for a 200-nm bead to diffuse away from the main field emitted by the aperture if it were in free Brownian motion (see below).

Figure 6 shows the fluorescence spectrum for an occupied hole as compared with the fluorescence spectrum in the absence of the metal film. The two spectra are normalized to the excitation light intensity ($\lambda = 400$ nm). An enhancement is apparent for the fluorescence coming from the nanochannel. Such enhancements have been predicted theoretically[24] and experimentally observed[17,20] for a variety of chromophores inside metallic wall nanoapertures. We thus infer that the enhancement in the fluorescence yield comes from regions of the particle immersed in the near-field of the nanochannel. The factor of 4 enhancement in Figure 6 is probably an underestimate since when the metal film is absent, the confocal microscope probes a ~20 μm^3 volume containing an average of 5 fluorescent beads; while in the case of the nanochannel, the fluorescence comes from a single bead. Thus, a more correct enhancement estimate should account for the larger number of particles contributing to the signal when the film is absent. These considerations lead to an enhancement factor of ~10. However, different regions of the depth of focus have different intensities, so this is just an approximate number.

While from Figures 5 and 6 it is clear that one can obtain particles immobilized inside laser-irradiated holes, the question is: what is the laser's role in this immobilization? This question can be addressed using our experimental setup by analyzing the fluorescence intensity fluctuations coming from a trapped bead. Assuming that the bead acts as a reporter for the local excitation field, the fluorescence intensity fluctuations come

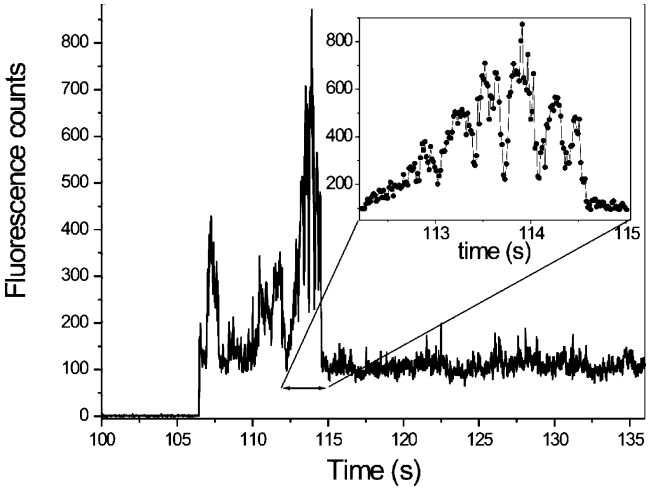

Figure 8. Fast recording (10 ms integration time) of fluorescence fluctuations occurring at the initial stages of trapping. Inset: close-up on a fluctuation exhibiting oscillations.

from two sources: (a) temporal fluctuations of the excitation field and (b) spatial fluctuations of the bead position within the excitation field. However, the laser fluctuations are totally uncorrelated even for the minimum time step that we use (5 ms). Hence, the only correlations that we can observe for a nonzero lag time will be set by the bead's motion.

We compare in Figure 7 the correlation functions of fluorescence intensity fluctuations under the same buffer and laser intensity conditions for a bead that is either trapped inside a hole or freely crossing the focus in the absence of a metal film. The widths of the two correlation functions differ by about an order of magnitude. Before analyzing these functions in detail we remark that for a motionless, adsorbed bead we expected (and observed) that the intensity correlation function vanishes (within measurement errors) for nonzero lag times. Hence, we may conclude that an entrapped bead is not adsorbed temporarily on the walls or silica top of the nanochannel for the duration of laser irradiation.

Now consider the correlation function for the free particle, which is determined by its diffusive motion across the laser focus.[25] With large spherical particles for which we can assume that the fluid sticks to the particle's surface, the diffusion coefficient is given by the Stokes−Einstein formula: $D = k_B T/6\pi\eta a$, where η is the shear viscosity of the fluid, a is the radius of the Brownian particle, T is the temperature, and k_B is Boltzmann's constant. For a sphere with $a = 100$ nm moving in water we obtain $D = 2.5 \times 10^{-8}$ cm^2/s. The correlation time, τ_{corr}, represents the average time required for the fluorescent particle to diffuse through the focus and is related to the diffusion coefficient by $\tau_{corr} = L^2/4D$, where L characterizes the transverse size of the focal spot.[25] From Figure 7 we extract $\tau_{corr} \approx 40$ ms. It then follows that $L \approx 0.6$ μm, which is comparable to the size of the diffraction limited spot. Hence, we have a consistent picture.

For trapped particles the interpretation is more difficult. Although it is evident from Figure 5 that particles can be trapped, the trapping process and final configuration are not clear. Faster recordings (5-ms resolution) of the initial stages of the trapping event seem to indicate that the bead explores at first for a short period of time different zones of the channel and then abruptly settles into a stable position, Figure 8.

The time before settling is characterized by strong and relatively slow fluorescence fluctuations, while the fluorescence after settling is characterized by rapid bursts and a slowly decaying baseline. An intriguing feature of the rapid bursts structure is its resemblance to a set of nested exponential decays, Figure 9. It is plausible that the location for stable trapping is at one of the "hot spots" on the edge of the nanochannel (Figure 9). However, it is not obvious how the particle approaches a stable location. The duration of the preliminary, slow wandering through the near-field intensity profile suggested by Figure 8 varies with each trapping event and often does not even occur.

To change the trapping conditions, we have added a second, near-infrared (NIR) laser ($\lambda = 800$ nm, 20−100 mW/mm^2) to vary the trapping forces, while maintaining the same excitation intensity for fluorescence. The extra field intensity suppressed the preliminary settling phase. The beads appeared to go immediately to the stable location with a modified spectrum of fluctuations. We observed that (1) the rate of the fluorescence bursts decreased with the NIR laser power, while (2) the decay time of these bursts increased. The behavior is as if the friction has been increased, perhaps because the stronger trapping forces are pulling the beads closer to a wall.

The variation of the correlation function with the near-infrared power was completely reversible, i.e., after turning the NIR beam off, the correlation function regained its initial shape. This feature indicates that sticking of the latex beads to the gold edges due to localized heating of the film is an improbable event both

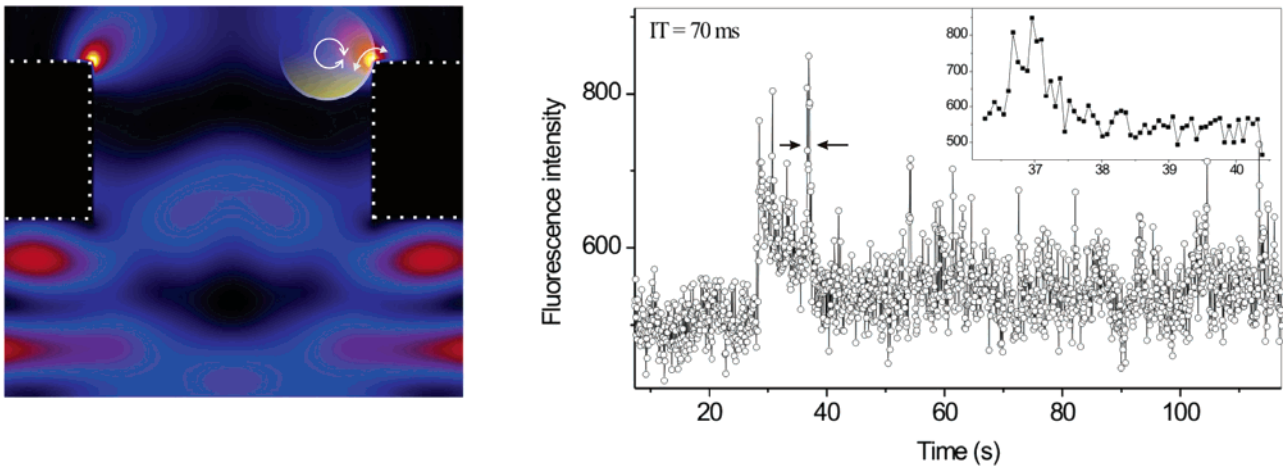

Figure 9. Left: numerical simulation of the cross-sectional light intensity with a sketch of the hypothetical trapping configuration on one of the near-field "hot" spots and possible degrees of freedom. The physical configuration is the same as in Figure 3. Fluorescence bursts from a settled, trapped bead look like nested exponentials (right). Inset: close-up of the burst marked by arrows.

because the laser power is significantly less than the reported values in previous sticking experiments [26] and because the observed sticking of latex beads on laser-heated scanning probes was irreversible,[26] in contrast to our findings. We do not exclude at this point the presence of thermal effects, although theoretical estimates of temperature changes due to similar laser intensities irradiating metallic scanning probe tips seem to indicate that they are negligible.[9] Moreover, turbulent thermal convection is less likely to occur at small spatial scales, which are characterized by small Rayleigh numbers.[27]

Similar to classical optical tweezers, it should be possible to estimate the optical trapping forces from the spectral analysis of intensity fluctuations in the scattered light.[6] Unfortunately, since the present detection is based on fluorescence, the useful bandwidth is limited by the fluorescence count rate at ~200 Hz. We have studied the spectral decomposition of fluorescence fluctuations for three NIR intensities (0, 40, and 100 mW/mm^2) with a constant (20 mW/mm^2) excitation power. Although it has not been possible to fit these spectral decompositions with a single Lorentzian function from which the oscillator constant could be extracted, we find that the 10-dB frequencies form a progression, indicating a trap stiffening that grows with the NIR intensity. Future experiments using transmission instead of fluorescence will take advantage of a larger bandwidth and the possibility of examining the entire spectral decomposition of time-dependent fluctuations, thus assessing the oscillator constant and its relationship with the trapping laser intensity, characteristics of the nanochannel trap, and surface preparation.

Conclusions

A proof-of-principle for near-field optical trapping with integrated apertures has been illustrated using fluorescent latex beads and lithographically fabricated nanochannels in metal films. Our results indicate that one can obtain near-field optical trapping with much lower intensity (~0.1 W/mm^2) than that required by classical optical tweezers (~10^3−10^4 W/mm^2). The theoretical analysis for the technique introduced here indicates that it should be possible to trap and study, one at a time, particles as small as 10 nm. The method could find applications in studies of microrheology in confined spaces because the particle/nanochannel system can be used as an optically addressable model with interfacial properties variable by design. Ultra-sensitive sensing of molecular binding events is another possible area of NFT application because of its unique features of reduced background, possibility of parallel addressing, and nanoscopic transducer size.

Acknowledgment. Support for this project comes from NSF grant BES 0322767. B.D. is thankful to Richard Martel for his comments regarding the manuscript.

References and Notes

(1) Ashkin, A. In *Single Molecule Spectroscopy*; Rigler, R., Orrit, M., Basche, T., Eds.; Springer: Berlin, 2002.
(2) Chu, S. *Rev. Mod. Phys.* **1998**, *70*, 685−706.
(3) Svoboda, K.; Block, S. M. *Annu. Rev. Biophys. Biomol. Struct.* **1994**, *23*, 247−285.
(4) Block, S. M. *Nature* **1992**, *360*, 493−495.
(5) Block, S. M. *Prog. Biophys. Mol. Biol.* **1996**, *65*, SH301−SH301.
(6) Bustamante, C.; Macosko, J. C.; Wuite, G. J. L. *Nat. Rev. Mol. Cell Biol.* **2000**, *1*, 130−136.
(7) Ashkin, A.; Dziedzic, J. M. *Science* **1987**, *235*, 1517−1520.
(8) Peterman, E. J. G.; Gittes, F.; Schmidt, C. F. *Biophys. J.* **2003**, *84*, 1308−1316.
(9) Novotny, L.; Bian, R. X.; Xie, X. S. *Phys. Rev. Lett.* **1997**, *79*, 645−648.
(10) Chaumet, P. C.; Rahmani, A.; Nieto-Vesperinas, M. *Phys. Rev. Lett.* **2002**, *88*, art. no. 123601.
(11) Chaumet, P. C.; Rahmani, A.; Nieto-Vesperinas, M. *Phys. Rev. B* **2002**, *66*, art. no. 195405.
(12) Calander, N.; Willander, M. *Phys. Rev. Lett.* **2002**, *89*, art. no. 143603.
(13) Xu, H. X.; Kall, M. *Phys. Rev. Lett.* 2002, 89, art. no. 246802.
(14) Levene, M. J.; Korlach, J.; Turner, S. W.; Foquet, M.; Craighead, H. G.; Webb, W. W. *Science* **2003**, *299*, 682−685.
(15) Taflove, A.; Hagness, C. *Computational Electrodynamics: The Finite-Difference Time-Domain Method*; Artech House: Boston, MA, 2000.
(16) Novotny, L.; Pohl, D. W.; Regli, P. *J. Opt. Soc. Am. A* **1994**, *11*, 1768−1779.
(17) Dunn, R. C. *Chem. Rev.* **1999**, *99*, 2891−2928.
(18) Jackson, J. D. *Classical Electrodynamics*; Wiley: New York, 1975.
(19) Dragnea, B.; Chen, C.; Kwak, E. S.; Stein, B.; Kao, C. C. *J. Am. Chem. Soc.* **2003**, *125*, 6374−6375.
(20) Fischer, U. C. *J. Opt. Soc. Am. B* **1986**, *3*, 1239−1244.
(21) Raether, H. *Surface Plasmons on Smooth and Rough Surfaces and on Gratings*; Springer-Verlag: Berlin, 1988.
(22) Ghaemi, H. F.; Thio, T.; Grupp, D. E.; Ebbesen, T. W.; Lezec, H. J. *Phys. Rev. B* **1998**, *58*, 6779−6782.
(23) Zhu, T.; Vasilev, K.; Kreiter, M.; Mittler, S.; Knoll, W. *Langmuir* **2003**, *19*, 9518−9525.
(24) Dereux, A.; Girard, C.; Weeber, J.-C. *J. Chem. Phys.* **2000**, *112*, 7775−7789.
(25) Berne, B. J.; Pecora, R. *Dynamic Light Scattering*; Dover: New York, 2000.
(26) Shivashankar, G. V.; Libchaber, A. *Appl. Phys. Lett.* **1997**, *71*, 3727−3729.
(27) Siggia, E. D. *Annu. Rev. Fluid Mech.* **1994**, *26*, 137−168.